Department of Physics and Astronomy

University of Heidelberg

Master thesis

in Physics

submitted by

Edoardo Rizzardi

born in Pavia

2018

Bound states

through

Imaginary frequency simulation

This Master thesis has been carried out by

Edoardo Rizzardi

at the

Institut für Theoretische Physik

under the supervision of

Prof. Dr. Jan Pawlowski

and

Prof. Dr. Alexander Rothkopf

ACKNOWLEDGMENTS

This work is the culmination of my experiences in Heidelberg, both academic and personal. Every person I've met and I care for contributed in my well-being, even though for a small part, and then to my project's, thus reserving acknowledgment and thanks. To all these people I dedicate my work.

I would like to firstly thank Alexander R. for his caring supervision and constant presence. Furthermore, Alexander L. with his insight and competence helped me with practical understanding of my project, his comments shed light on many of my doubts, and his personal support (physics jokes apart) contributed to the success of my master thesis.

Special thanks go to my fellow physics students, whose struggles made me understand that I am not alone with mines.

Huge love is deserved by the "italian gang" and the "spanish team". Countless hours spent together cooking, eating and listening to bad music truly reshaped the meaning of "affection". Of course, friendship is not bound by nationality: so all my friends, regardless of their origin, deserve my sincere gratitude.

Not to forget the SAI students, whose inexplicable connection with physics students produced some of my most precious moments in Heidelberg.

Even across hundreds kilometers of distance, my long term friends from Bressana (a.k.a. "i Postribolari"), always reminded me my connection to my small countryside hometown.

Finally, I thank my parents and my sister, for all the years of mutual love and support. All of this would not have happened without you.

ABSTRACT

In this work we give numerical evidence the existence of bound states in the broken phase of 2+1 dimensional real scalar φ^4-theory. The result is achieved using a novel simulation prescription based in imaginary frequencies in order to obtain correlator $G(\omega) = \langle \varphi(\omega)\varphi(-\omega)\rangle$. Subsequently, spectral functions are extracted from correlator data using Bayesian spectral reconstruction.

ZUZAMMENFASSUNG

Diese Arbeit untersucht die reale skalare φ^4-Theorie in 2+1 Raumzeitdimensionen. Unter Nutzung einer neuartigen Simulationsmethode werden die Korrelationsfunktionen $G(\omega) = \langle \varphi(\omega)\varphi(-\omega) \rangle$, direkt im Frequenzraum bestimmt. Anschließend werden mithilfe der bayesischen Rekonstruktionsmethode die Spektralfunktionen extrahiert

CONTENTS

INTRODUCTION

Bound states are localized systems of two or more particles. They play an important role in a wide variety of phenomena. For example, in particle physics a quark and antiquark can form quarkonium bound state; in condensed matter physics, the equivalent of the electron fluid of a superconducting material is understood as a fluid of Cooper pairs, namely bound states composed of two electrons. In quantum mechanics identifying bound states is a well understood: solving the Schrödinger equation in the presence of a potential allows direct study of bound states, identifying them as the negative-energy eigenstates of the Hamiltonian; bound states are univoquely identified as a vector in the single-particle Fock space of the Hamiltonian governing the system. In quantum field theory, instead, the Fock space representation is possible only for free theories, bound states appear only in interacting theories. So identifying the bound states in quantum field theory becomes a problem.

An unambiguous sign for the presence of a bound state can be seen in the spectral function of the connected two point funtion in imaginary time $G(\tau) = \langle \varphi(\tau)\varphi(0)\rangle_c$. It shows singularities at frequency values corresponding to the ground state energy, the ground state mass of the field, and to excited states enegy, e.g. the mass of bound states. Also, a shift of the peaks to the lower frequency part of the spectrum can be observed in presence of bound states. The imaginary time, and its Fourier transform $G(\omega) = \langle \varphi(\omega)\varphi(-\omega)\rangle_c$, are related to the spectral function via convolution over, respectively, a Laplace and a Källén-Lehmann kernel [1].

The 2+1-dimensional real scalar φ^4 theory shows a bound state in the symmetry broken phase [2]. The mass ratio between the bound state and the ground state mass was computed using, among other methods, non-perturbative renormalization group

[3] and numerical diagonalization methods [4]. Both studies found a mass ratio between the bound state and the ground state of $M/m \approx 1.8$. Close to criticality, the scalar φ^4 theory belongs to the 2D Ising model universality class, and Monte Carlo simulations of the Ising model at temperature lower than T_c showed a bound state with mass ratio $M/m \approx 1.8$ [5]. Thus, the existence of this bound state is a well-known fact. Higher bound states are also present, as shown by the complete determination of the bound state spectrum of the 2D Ising model [6].

The aim of this work is to study this phenomenon using as a starting point a novel simulation prescription for lattice field theory [7]. It is a Monte Carlo simulation algorithm based on a careful distinction between dynamics and initial conditions. This method and aims to resolve the problem that plagues the standard prescription for lattice simulations: since fields are simulated on a compact imaginary-time domain, their Fourier transform is discretized, i.e. defined only on the Matsubara frequencies $\omega_n = 2\pi nT$, thus structurally limiting resolution on observables. This new prescription allows for arbitrary resolution, limited only by computational resources.

Spectral functions are then extracted from correlator data using a spectral reconstruction algorithm based on Bayes theorem. The algorithm aims to select the most probable spectral function given incomplete and noisy Monte Carlo simulation results. It is based on the maximization of the posterior probability, that is the conditional probability of having a spectral function given correlator data. We aim to read clues of the existence of the first bound state in the real scalar φ^4 theory from the spectral function, extracted from simulated correlator data in the broken symmetry phase.

This work is structured as follows: in chapter 1 we lay the theoretical background necessary to tackle the problem; in chapter 2 we present the imaginary frequency prescription with detail of implementation; in chapter 3 bayesian spectral reconstruction and its numerical details are explained. These method

are used to gather numerical evidence for the existence of bound states in the symmetry broken phase of the real scalar φ^4 theory. We discuss our results our results and compare to previous estimates form the literature in chapter 5.

1

THEORETICAL INTRODUCTION: THERMAL FIELD THEORY

SCHWINGER-KELDYSH CONTOUR

The starting point of the theoretical description underlying our work is the one of real-time thermal field theory. It relies on general concepts of statistical mechanics and quantum field theory, and will be explained in this chapter. This exposition follows [8].

The expectation value of an observable $\hat{O}$ evaluated in a statistical ensemble, with each state $|\phi_k\rangle$ having probability p_k is

$$\left\langle \hat{O} \right\rangle = \sum_k p_k \left\langle \phi_k \right| \hat{O} \left| \phi_k \right\rangle \; = \; \mathrm{Tr} \left\{ \hat{\rho} \, \hat{O} \right\}, \tag{1.1}$$

with $\hat{\rho}$ density operator, which fulfills

$$\hat{\rho} = \sum_k p_k \left| \phi_k \right\rangle \left\langle \phi_k \right|, \tag{1.2a}$$

$$\mathrm{Tr}\hat{\rho} = 1. \tag{1.2b}$$

In general, the density operator can be time-dependent. Its time evolution is described by the von Neumann equation:

$$\partial_t \hat{\rho} = -\frac{i}{\hbar} \left[\hat{H}, \hat{\rho} \right]. \tag{1.3}$$

This is the quantum equivalent of the classical Liouville equation.

The von Neumann equation has a well known solution, that makes use of the unitary time evolution operator $\hat{\mathcal{U}}(t, t_0)$:

$$\hat{\rho}(t) = \hat{\mathcal{U}}(t, t_0) \hat{\rho}(t_0) \hat{\mathcal{U}}(t_0, t) \tag{1.4}$$

where the time evolution operator is solution of the euqation

$$\partial_t \hat{\mathcal{U}}(t, t_0) = -\frac{i}{\hbar}\hat{\mathcal{U}}(t, t_0). \tag{1.5}$$

Starting from some given initial density matrix $\hat{\rho}(t_0)$, the computation of a time-dependent expectation value of an observable O then involves

$$\left\langle \hat{O}(t) \right\rangle = \mathrm{Tr}\left\{\hat{O}\hat{\rho}(t)\right\} = \mathrm{Tr}\left\{\hat{\mathcal{U}}(t, t_0)\hat{O}\hat{\mathcal{U}}(t_0, t)\hat{\rho}(t_0)\right\}. \tag{1.6}$$

The invariance of the trace under cyclical permutations of the arguments was used. This expression describes an evolution from t_0, where the initial density operator is specified, towards t, where the observable is calculated, and then back to the initial time. This evolution is said to take place on a "closed time path" $\mathcal{C}$.

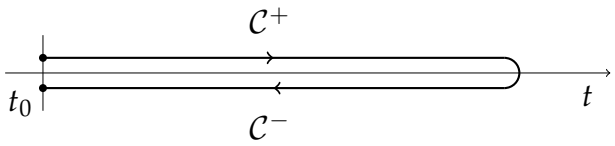

Figure 1: Real time closed path $\mathcal{C} = \mathcal{C}^+ + \mathcal{C}^-$. The two branches are separated for visualization purposes.

Restricting ourselves to thermal equilibrium, the density operator must obey the equation (for a time-independent $\hat{H}$)

$$\partial_t \hat{\rho}|_{\hat{\rho}=\hat{\rho}^{eq}} = -\frac{i}{\hbar}\left[\hat{H}, \rho^{\hat{e}q}\right] \stackrel{!}{=} 0. \tag{1.7}$$

This condition is realized for all density operators that depend only on conserved quantities, i.e. energy $\hat{H}$ or particle number $\hat{N}$. Those operators correspond to the statistical ensembles

$$\begin{aligned} \text{canonical: } \hat{\rho}^{eq} &= \frac{e^{-\beta\hat{H}}}{\mathrm{Tr}e^{-\beta\hat{H}}}, \\ \text{grand canonical: } \hat{\rho}^{eq} &= \frac{e^{-\beta(\hat{H}-\mu\hat{N})}}{\mathrm{Tr}e^{-\beta(\hat{H}-\mu\hat{N})}}; \end{aligned} \tag{1.8}$$

with $\beta = \frac{1}{k_B T}$.

For a time-independent Hamiltonian, the unitary time evolution operator is explicitly given by

$$\hat{\mathcal{U}}(t, t_0) = e^{-\frac{i}{\hbar}\hat{H}(t-t_0)} \tag{1.9}$$

Performing a Wick rotation $t \to -i\bar{\tau}$ one can define *imaginary time* Heisenberg operators

$$\hat{O}(\bar{\tau}) = e^{\hat{H}\bar{\tau}}\hat{O}e^{-\hat{H}\bar{\tau}} \tag{1.10}$$

The name "imaginary time" comes from the fact that the time-variable is actually imaginary: the temporal axis has been rotated 90° into the complex plane. Let us consider the canonical density matrix $\hat{\rho}^{eq} \sim e^{-\beta\hat{H}}$, then this operator is the euclidean version of the time evolution operator, with $\beta\hbar \equiv \bar{\tau} = it$. Thus, observing in this new prespective the expectation value at thermal equilibrium of an observable (starting from the initial time $t_0 = 0$)

$$\begin{aligned} \left\langle \hat{O}(t) \right\rangle &= \mathrm{Tr}\left\{ e^{-\beta\hat{H}}\hat{O}(t) \right\} = \\ &= \mathrm{Tr}\left\{ e^{-\beta\hat{H}} e^{\frac{i}{\hbar}\hat{H}t}\hat{O}e^{-\frac{i}{\hbar}\hat{H}t} \right\}. \end{aligned} \tag{1.11}$$

This equation, as stated before, involves a time path from $t_0 = 0$ to t, where the operator is evaluated, and then a backwards evolution again to t_0. This evolution takes place on the aforementioned closed time path. But the presence of the canonical density matrix extends this time path into the imaginary time axis: it adds a third branch, from t_0 to $t_0 - i\hbar\beta$:

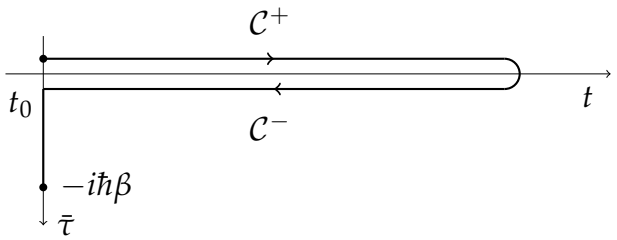

Figure 2: Schwinger-Keldysh contour.

This new time path is called *Schwinger-Keldish contour*. The construction of the Schwinger-Keldish contour is possible *only*

because we are in thermal equilibrium: in general, at non-equilibrium the density operator cannot be seen as an imaginary-time evolution operator, thus the evolution happens only in the real-time closed contour $\mathcal{C}$.

Using the path integral approach to quantum mechanics [1], expectation values (1.1) can be conputed via the formula

$$\left\langle \hat{O}(t) \right\rangle = \frac{\int Dq\, O(t) e^{-S(t)}}{\int Dq\, e^{-S(t)}}; \tag{1.12}$$

where the action is (in Euclidean spacetime):

$$S(t) = \int_{\mathcal{C}} dt\, \mathcal{L}(t). \tag{1.13}$$

The integral $\int_{\mathcal{C}} dt$ means that is performed on the closed timepath $\mathcal{C}$.

Remembering the fact that quantum mechanics is quantum field theory in $0+1$ dimensions, the qft, i.e. the $d+1$-dimensional version of (1.12) is

$$\left\langle \hat{O}[\Phi] \right\rangle = \frac{\int Dq\, O[\Phi] e^{-S[\Phi]}}{\int Dq\, e^{-S[\Phi]}}, \tag{1.14}$$

and the action reads:

$$S[\Phi] = \int_{x,\mathcal{C}} dx\, \mathcal{L}[\Phi] = \int_{\mathcal{C}} dx^0 \int d^d x\, \mathcal{L}[\Phi]. \tag{1.15}$$

GENERATING FUNCTIONAL

All the informations of a general quantum field theory, in and out of equilibrium, are encoded in its generating functional, the partition function, amended by source terms $J(x)$

$$\mathcal{Z}[\Phi, J] = \mathrm{Tr}\left\{ \rho T_{\mathcal{C}}\; e^{\int_{x,\mathcal{C}} dx\, \Phi(x) J(x)} \right\}, \tag{1.16}$$

where $T_{\mathcal{C}}$ corresponds to the usual time ordering operator along the forward branch $\mathcal{C}^+$ and reverse ordering on the backwar one $\mathcal{C}^-$. Through functional differentiation of (1.16) one can obtain correlation functions, for example the one point function reads:

$$\left. \frac{\delta \mathcal{Z}[\Phi, J]}{i \delta J(x)} \right|_{J=0} = \mathrm{Tr}\{\rho_0 \Phi(x)\} = \langle \Phi(x) \rangle := \phi(x). \tag{1.17}$$

Similarly, time-ordered two-point functions can be obtained with two functional differentiations:

$$\left.\frac{\delta^2 \mathcal{Z}[\Phi, J]}{i\delta J(x) i\delta J(y)}\right|_{J=0} = \mathrm{Tr}\left\{\rho_0 T_{\mathcal{C}} \Phi(x)\Phi(y)\right\} = \left\langle T_{\mathcal{C}} \Phi(x)\Phi(y)\right\rangle . \tag{1.18}$$

Definig the connected two point function as:

$$G(x,y) = \left\langle T_{\mathcal{C}} \Phi(x)\Phi(y)\right\rangle - \phi(x)\phi(y), \tag{1.19}$$

(1.18) becomes:

$$\left\langle T_{\mathcal{C}} \varphi(x)\varphi(y)\right\rangle = G(x,y) + \phi(x)\phi(y). \tag{1.20}$$

To iprove the notation, one can use the superscript $\pm$ on the field $\Phi^{\pm}$ to explicitly denote on which branch of the contour $\mathcal{C}$ the variable x^0 is located. The linear source term in (1.16) then becomes:

$$\begin{aligned}\int_{x,\mathcal{C}} dx\, \Phi(x)J(x) &= \int_{t_0}^{\infty} dx^0 \int d^d x\, \Phi^+(x)J^+(x) + \\ &+ \int_{\infty}^{t_0} dx^0 \int d^d x\, \Phi^-(x)J^-(x) = \\ &= \int_{t_0}^{\infty} dx^0 \int d^d x (\Phi^+(x)J^+(x) - \Phi^-(x)J^-(x)).\end{aligned} \tag{1.21}$$

Differentiating the generating functional with respect to each of the source terms give always the same one point function:

$$\left.\frac{\delta \mathcal{Z}[\Phi, J]}{i\delta J^+(x)}\right|_{J^+=0} = \left.\frac{\delta \mathcal{Z}[\Phi, J]}{i\delta J^-(x)}\right|_{J^-=0} = \phi(x), \tag{1.22}$$

because time ordering doesn't matter for one-point function. Taking now the second functional derivative of the generating functional with respect to J^+ we obtain:

$$\left.\frac{\delta^2 \mathcal{Z}[\Phi, J]}{i\delta J^+(x) i\delta J^+(y)}\right|_{J=0} = G^{++}(x,y) + \phi(x)\phi(y). \tag{1.23}$$

Identical results can be obtained by differentiating with respect to both sources J^+ and J^-, involving the two-point functions G^{+-}, G^{-+} and G^{--}.

Path integral representation

By writing the trace as a sum on $|\varphi^{\pm}\rangle$ eigenstates of the field operator $\Phi^{\pm}$ at the initial time t_0, one can formulate the generating functional (1.16) in a path integral form:

$$\mathcal{Z}[J,\rho_0,\Phi] = \underbrace{\int [d\varphi_0^+][d\varphi_0^-]\,\langle\varphi^+|\rho_0|\varphi^-\rangle}_{\text{initial conditions}} \times \underbrace{\int_{\varphi_0^+}^{\varphi_0^-} \mathcal{D}\Phi\, e^{-iS_M[\Phi^+]-iS_M[\Phi^-]}}_{\text{quantum dynamics}}. \tag{1.24}$$

This equation contains two important ingredients of the theory: first, the initial conditions, which are encoded in the averaging over the density operator elements; second, quantum fluctuations described by the path integral over field configurations Φ on the branches of the closed time contour in Fig. 2. This is the general non-equilibrium path-integral representation of the partition function. As noted before, in thermal equilibrium one can identify the initial density operator as an ensemble density operator, i.e. an imaginary-time evolution operator. Thus, at thermal equilibrium the partition function becomes:

$$\mathcal{Z}[J,\rho_0,\Phi] = \underbrace{\int_{\Phi_E(0)}^{\Phi_E(\beta)} \mathcal{D}\Phi\, e^{-S_E[\Phi_E]}}_{\text{initial conditions}} \times \underbrace{\int_{\Phi^+(t_0,x)}^{\Phi^-(t_0,x)} \mathcal{D}\Phi\, e^{-iS_M[\Phi^+]+iS_M[\Phi^-]}}_{\text{quantum dynamics}}. \tag{1.25}$$

Equation (1.25) can be read as follows: an integration in imaginary time $\bar{\tau}$ over all thermal field configurations Φ with distribution $e^{-S_E[\Phi]}$ provides the boundary values for an integration over the real-time-contour $\mathcal{C}$ with weight $e^{-iS_M[\Phi^+]+iS_M[\Phi^-]}$.

2

IMAGINARY FREQUENCY SIMULATION

In the previous chapter the Schwinger-Keldysh contour was introduced. It was used to define the expectation value of observables at thermal equilibrium. Numerical evaluation of the path integral (1.14) are often based on non-perturbative Monte Carlo methods [9]. Moving from the continuum description to one more suitable for numerical computations, the path integral has to be defined on a subset of the configuration space, and the action is to be discretized such that it lives on an isotropic lattice Λ, with lattice spacing a. Given the very large number of degrees of freedom, then one has to resort to Monte Carlo simulations: generate randomly field configurations in the space of field configurations, and then explicitly calculate the action. Altough possible, this method is somehow extremely siplified and inefficient: the integrand of the path integral is peaked around a specific field configuration, the one that maximizes the action. Thus drawing randomly from field configuration space becomes computationally intensive, and meaningful outcomes are higly costly. Instead, one can resort to importance sampling: drawing field configurations such that their distribution follows $e^{-S[\phi]}$. This comes with an improvement in accuracy and computation time, since the important configuration are more likely to be drawn.

This task consists of generating a large number N of configurations $\{\phi_n; n = 1, 2, ..., N\}$ drawn in the vicinity of the configuration that maximizes the action, so that the distribution of this sample approximates the desired distribution. The Monte Carlo-time average is then taken to compute expectation values

$$\langle O(\phi) \rangle = \frac{1}{N} \sum_{n=1}^{N} O(\phi_n), \tag{2.1}$$

for $N \gg 1$.

Many Monte Carlo algorithms based on importance sampling are available (see e.g. [10]), we opted for stochastic quantization [11].

STOCHASTIC QUANTIZATION

Stochastic quantization is a kind of importance sampling based Monte Carlo technique. It relies on constructing a "fictitious" Wiener-Markoff stochastic process, evolving in Monte Carlo time s, such that its equilibrium distribution is $\Phi[\phi] \sim e^{-S[\phi]}$. Field configurations are then drawn as istantaneous configurations of the stochastic process.

A Wiener-Markoff stochastic process with n degrees of freedom can be described by the Langevin equation:

$$\frac{dq_i}{ds} = K_i(q(s)) + \eta_i(s), \text{ with } i = 1, ..., n; \tag{2.2}$$

with $q_i(s)$ being the variables describing the system, $K_i(q(s)) = -\frac{\partial V(q)}{\partial q_i}$ the drift force (total instantateous force) and $\eta_i(s)$ the random forces, represented by white Gaussian noise, such that:

$$\langle \eta_i(s) \rangle = 0, \tag{2.3a}$$

$$\langle \eta_i(s)\eta_j(s') \rangle = 2\alpha\delta_{ij}\delta(s - s'). \tag{2.3b}$$

At thermal equibrium, the stochastic process has a stationary distribution, i.e. there exists a distribution $\Phi(q, s)$ such that:

$$\int O(q)\Phi(q, s)dq = \langle O(q(s)) \rangle , \; dq = \prod_i dq_i$$

From this equality one can derive the Fokker-Planck equation:

$$\frac{\partial \Phi(q, s)}{\partial s} = F\Phi(q, s) \tag{2.4a}$$

$$F = \sum_i \left[\alpha \frac{\partial^2}{\partial q_i^2} + K_i(q) \frac{\partial}{\partial q_i} \right]. \tag{2.4b}$$

F being the Fokker-Planck operator. At thermal equilibrium, (2.4) becomes:

$$\frac{\partial}{\partial s}\Phi_{eq}(q,s) = 0 \tag{2.5}$$

or

$$\sum_i \left[\alpha\frac{\partial^2}{\partial q_i^2} + K_i(q)\frac{\partial}{\partial q_i}\right]\Phi_{eq}(q,s) = 0. \tag{2.6}$$

Being $K_i(q) = -\frac{\partial V(q)}{\partial q_i}$, (2.6) has the solution:

$$\Phi_{eq}(q) = C\exp\left\{-\frac{V(q)}{k_B T}\right\}. \tag{2.7}$$

So, choosing the drift force appropriately, one can find a distribution that provides the same expectation values as the quantum field theory one wants to describe. This feature is the central point of stochastic quantization: if one chooses the drift force to be

$$K_i(q(s)) = -\left(\frac{\partial S[q]}{\partial q_i}\right), \tag{2.8}$$

with $S[q]$ the action of the field theory of choice, one finds immediately that the stationary distribution is:

$$\Phi_{eq}[q] = C\exp\left[-\frac{1}{\alpha}S[q]\right]. \tag{2.9}$$

The Feynman path integral measure comes directly if one imposes the drift constant to be $\alpha = \hbar$.

In field theory, the coordinates q are field configurations, defined on space-time coordinates $(t, \mathbf{x})$, and thus, after all the considerations above, the resulting Langevin equation is

$$\frac{d\Phi_i(t,\mathbf{x};s)}{ds} = -\frac{\delta S[\Phi]}{\delta\Phi(t,\mathbf{x};s)} + \eta_i(t,\mathbf{x};s). \tag{2.10}$$

Expectation values for observable computed through (2.10) will then correspond to the one computed with the path integral (1.14).

LANGEVIN SOLUTION

In order to use stochastic quantization as a Monte Carlo algorithm, one has to solve numerically the Langevin equation (2.10). The starting point is to discretize the action of the chosen field theory. In this work we study real scalar field theory, so we refer to the action in Euclidean signature

$$S = \int d^d x \left(\frac{1}{2} \partial_\mu \varphi_E \partial_\mu \varphi_E + \frac{1}{2} m^2 \varphi_E^2 + \frac{\lambda}{4!} \varphi_E^4 \right) \tag{2.11}$$

Moving to a periodic and isotropic lattice $\Lambda = N_\omega \times N_p^{d-1}$ points, with uniform spacing a, the action discretizes as follows

$$S_\Lambda = a^3 \sum_{x \in \Lambda} \left(-\frac{1}{2} \varphi_x \Delta \varphi_x + \frac{1}{2} m^2 \varphi_x^2 + \frac{\lambda}{4!} \varphi_x^4 \right), \tag{2.12}$$

where $\Delta \varphi_x := \sum_\mu (\varphi_{x+\hat{\mu}} + \varphi_{x-\hat{\mu}} - 2\varphi_x)/a^2$ is the discrete Laplacian. The last equation is a result of a partial integration of the action in the presence of periodic boundary conditions on the lattice.

The Langevin equation (2.10) is solved using a second order Runge-Kutta method [12], [13]. The configuration at the timestep $s+1$ is (with timestep δs):

$$\varphi_x^{s+1} = \varphi_x^s - \frac{\delta s}{2} \left(\nabla S_x^s + \nabla S_x^{s+1/2} \right) + \sqrt{\delta s} \eta_x. \tag{2.13}$$

$\nabla S_x^s := \frac{\delta S}{\delta \varphi_x}^s$ and $\nabla S_x^{s+1/2} := \frac{\delta S}{\delta \varphi_x}^{s+1/2}$ are the drift evaluated respectively at time s and $s+1$, given by

$$\nabla S_x^s = m \varphi_x^s - \Delta \varphi_x^s + \frac{\lambda}{6} (\varphi_x^s)^3, \tag{2.14}$$

$$\nabla S_x^{s+1/2} = m \varphi_x^{s+1/2} - \Delta \varphi_x^{s+1/2} + \frac{\lambda}{6} (\varphi_x^{s+1/2})^3; \tag{2.15}$$

with $\varphi_x^{s+1/2}$ being

$$\varphi_x^{s+1/2} = \varphi_x^s + \frac{\Delta s}{2} \nabla S_x^s + \sqrt{\frac{\Delta s}{2}} \eta_x. \tag{2.16}$$

It is crucial to note that the Gaussian noise in (2.13) and (2.16) is the same.

To use stochastic quantization as a Monte Carlo algorithm, one has to follow the procedure:

1. Generate a series of field configurations at thermal equilibrium by solving Langevin equation. Each configuration $\varphi_n = \varphi(s_n)$ is a solution at a specific timestep s_n;
2. Use generated configuration to calculate physical observables $O^n = O(\varphi_n)$;
3. Compute quantum expectation values by calculating the long-time average

$$\frac{1}{n}\sum_{i=0}^{n-1} O(\varphi(s_i)) \approx \int \mathcal{D}\varphi O(\varphi) e^{-S[\varphi]}, \text{ for } n \gg 1. \quad (2.17)$$

SIMULATION PRESCRIPTION

As noted in the introduction, resolution on observables computed using the standard simulation prescription is structurally limited by the Matsubara frequencies. Furthermore, increasing the number of points N_τ in the imaginary time axis one does not improve resolution, but increase the number of Matsubara frequencies available, keeping the spacing between frequencies fixed. Fig. 3 shows this feature. The plots were obtained through a standard simulation of a free 2+1-dimensional real scalar field on a discretized real-time axis, with $N_\tau = 8$ and $N_\tau = 16$ points on the discretized imaginary-time direction. Temperature was fixed to 1, in units of $\hbar/k_b$. The observable computed is the Fourier transform of (1.19), $G(\omega) = \langle \varphi(\omega)\varphi(-\omega)\rangle$. For details about the simulation prescription we refer to [9]. As one can see, increasing the number of points on the discretized imaginary-time axis doesn't inrease resolution on observables defined in Fourier space, but only gains access to higher Matsubara frequencies.

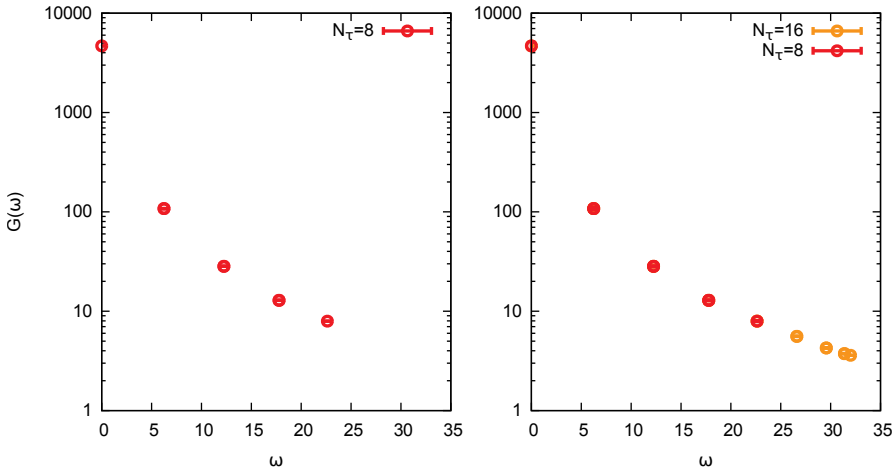

Figure 3: Left: correlator simulated on a $N_\tau = 8$ lattice. Right: same observable, simulated on a $N_\tau = 16$ lattice.

The newly proposed algorithm [7] allows for arbitrary resolution between Matsubara frequencies, by simulating directly in imaginary frequency space.
The problem is formulated as an initial value problem on the Schwinger-Keldysh contour, with the path integral representation for the partition function (1.25). The main idea behind the method is that of simulating directly in the Wick-rotated real-time contour, on an imaginary-time axis τ different from the initial conditions one. Since we are in thermal equilibrium, the real time contour branch can extend to infinity. Also, correlations between $t = +\infty$ and finite t vanis, thus we are allowed to cut the real time contour branch open at $t = +\infty$, and then Wick-rotate the two now separated branches the axis τ; the forward branch in the upper complex plane, the backward branch in the lower one.

In thermal equilibrium, the correlator in (3.4) is the analytic continuation of the Fourier transform of the imaginary-time connected correlator

$$G^{++}(\tau, \mathbf{p} = 0) = \sum_{\mathbf{x}} \left(\left\langle \varphi^+(\tau, \mathbf{x}) \varphi^+(0,0) \right\rangle - \left\langle \varphi^+(\tau, \mathbf{x}) \right\rangle \left\langle \varphi^+(0,0) \right\rangle \right) = \\ = \sum_{\mathbf{x}} \left(\left\langle \varphi^+(\tau, \mathbf{x}) \varphi^+(0,0) \right\rangle - \left\langle \varphi^+(0, \mathbf{x}) \right\rangle \left\langle \varphi^+(0,0) \right\rangle \right), \tag{2.18}$$

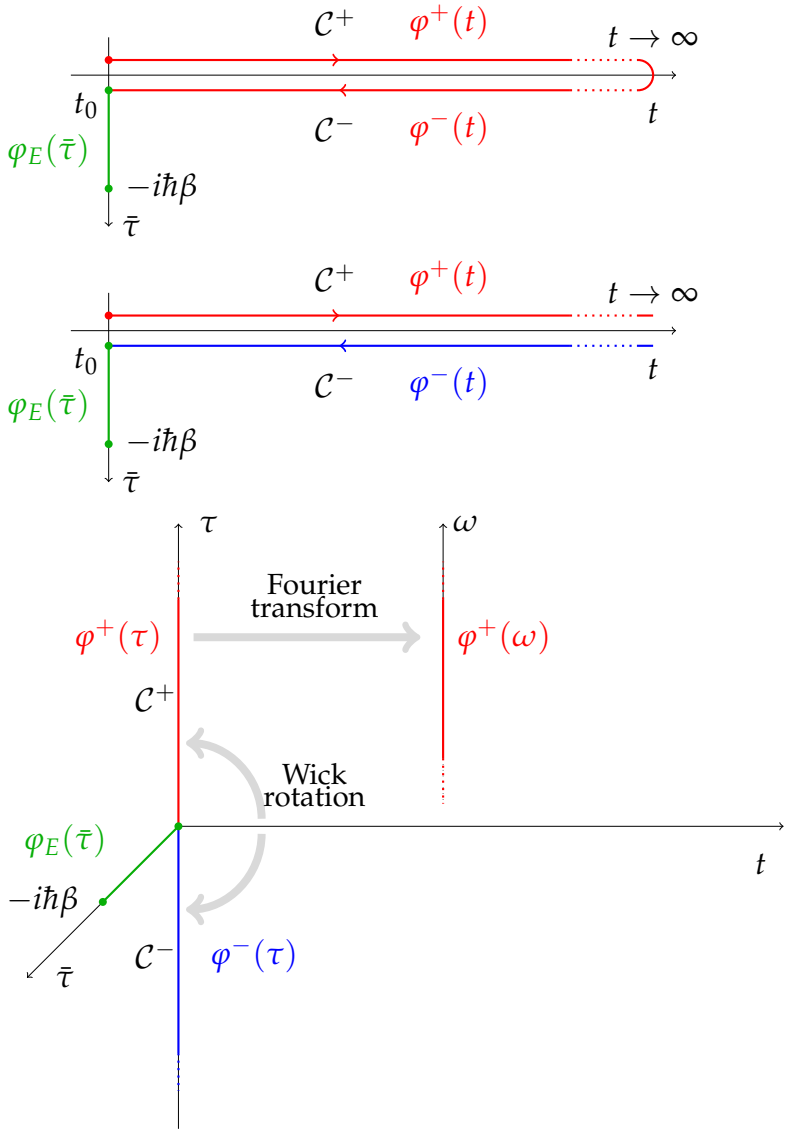

Figure 4: Construction scheme of the time contour for the imaginary frequency siulation prescription. Top: taking the limit $t \to \infty$. Center: cutting of the branches at $t = \infty$ (different colors were used to emphasize the fact that now $\mathcal{C}^+$ and $\mathcal{C}^-$ are not anymore connected). Bottom: Wick-rotation of each of the branches separately, to the imaginary-time axis $\tau \neq \bar{\tau}$. The simulation occurs in the rotated $\mathcal{C}^+$, then Fourier-transformed.

(the last equality holds for translational invariance of the one-point function) that is

$$\tilde{G}^{++}(\omega, \mathbf{p}=0) = \mathcal{F}_\tau G^{++}(\tau, \mathbf{p}=0) = \\ = \left\langle \varphi^+(\omega)\varphi^+(-\omega) \right\rangle - \sum_{\mathbf{x}} \left\langle \varphi^+(0,\mathbf{x}) \right\rangle \left\langle \varphi^+(0,0) \right\rangle \delta(\omega). \tag{2.19}$$

We thus need to simulate on the forward branch, discarding the backwards one. Fields on the forward branch are simulated via solving the Langevin equation

$$\partial_s \varphi^+(\tau, \mathbf{x}; s) = -\frac{\delta S[\varphi^+]}{\delta \varphi^+(\tau, \mathbf{x}; s)} + \eta(\tau, \mathbf{x}; s), \tag{2.20}$$

and initial conditions are simulated on the compact imaginary-time domain via solving the equation

$$\partial_s \varphi_E(\bar{\tau}, \mathbf{x}; s) = -\frac{\delta S[\varphi_E]}{\delta \varphi_E(\bar{\tau}, \mathbf{x}; s)} + \eta(\bar{\tau}, \mathbf{x}; s), \tag{2.21}$$

and imposed via

$$\varphi^+(\tau = 0) = \varphi_E(\bar{\tau} = 0). \tag{2.22}$$

OBSERVABLE COMPUTATION

The interesting observable for our purpouse is (2.19). The analytical continuation of its Fourier transform (2.18) in the free theroy behaves as

$$G(\tau) \propto e^{-m|\tau|}. \tag{2.23}$$

It is real, and, being defined on a periodic domain, is also periodic. Both features are present also in its lattice equivlent, so (2.19) is real. Then, one needs to compute only

$$\mathrm{Re}G^{++}(\omega) = \left\langle \mathrm{Re}\varphi^+(\omega)\mathrm{Re}\varphi^+(-\omega) - \mathrm{Im}\varphi^+(\omega)\mathrm{Im}\varphi^+(-\omega) \right\rangle + \\ - \sum_{\mathbf{x}} \left\langle \varphi^+(0,\mathbf{x}) \right\rangle \left\langle \varphi^+(0) \right\rangle \delta_{\omega 0}. \tag{2.24}$$

The expectation value is to be interpreted in the stochastic quantization sense: several realizations of the observable are measured, for each drawn field configuration. At the step i the

field $\varphi^{+(i)}(\omega)$ is drawn by solving (2.10) after imposing initial conditions via (2.22), and the $i-$th realization of the observable is calculated

$$\begin{aligned}\mathrm{Re}G^{++(i)}(\omega) = \mathrm{Re}\varphi^{+(i)}(\omega)\mathrm{Re}\varphi^{+(i)}(-\omega) - \mathrm{Im}\varphi^{+(i)}(\omega)\mathrm{Im}\varphi^{+(i)}(-\omega) + \\ - \sum_{\mathbf{x}} \varphi^{+(i)}(0,\mathbf{x})\varphi^{+(i)}(0)\delta_{\omega 0}.\end{aligned} \tag{2.25}$$

So, each of the $\varphi^{+(i)}(\omega)$ is an individual field configuration drawn from configuration space. Each of the $\mathrm{Re}G^{++(i)}(\omega)$ is an individual measurement of the correlator. The path integral expectation value is the Monte Carlo-time average of each of these measurements

$$\frac{1}{M}\sum_{i=0}^{M-1} G^{++(i)}(\omega) \approx G(\omega), \tag{2.26}$$

for $M \gg 1$.

To recap, the algorithm for imaginary frequency simulation can be summarized as follows

1. Update field $\varphi_E(\bar{\tau})$ on compact imaginary-time domain $\bar{\tau}$ trough Langevin equation and draw field configuration $\varphi_E^{(i)}(\bar{\tau})$;
2. Impose initial conditions by substituting $\varphi_E(\bar{\tau} = 0) \equiv \varphi^{+}(\tau = 0)$;
3. Update the field $\varphi^{+}(\tau)$ on the Wick-rotated real-time axis τ and draw field configuration $\varphi^{+(i)}(\tau)$;
4. Fourier-transform $\varphi^{+(i)}(\tau)$ to $\varphi_{\omega}^{+(i)}$ and calculate single realization of an observable (2.25);
5. Compute quantum expectation value via Monte Carlo-time average $\langle G(\omega)\rangle \approx \frac{1}{M}\sum_{i=1}^{M-1} G^{++(i)}$.

Measurement and autocorrelation

Drawing a new configuration by alterating the previous one by a single Langevin update leaves them to be quite similar,

thus introducing autocorrelation along Monte Carlo-time. A problem that plagues every kind of Monte Carlo simulation. Autocorrelation is quantitatively expressed by the formula [14]

$$A_i(\delta s) = \left\langle (G_i^{(j)} - \bar{G}_i)(G_i^{(j+\delta s)} - \bar{G}_i) \right\rangle \tag{2.27}$$

that is the correlation of two measurements as function of the Monte Carlo-time lag δs. Actually, this definition is very inefficient computationally wise for large samples. The calculation was performed using the convolution theorem. The convolution product (2.27) is a pointwise product in Fourier space. Denoting with $\mathcal{F}$ the Fourier transform, the new "practical" definition reads

$$A_i(\delta s) = \mathcal{F}^{-1}\left\{ \mathcal{F}\left\{G_i(\delta s) - \bar{G}_i\right\} \cdot \mathcal{F}\left\{G_i(\delta s) - \bar{G}_i\right\}^* \right\} \tag{2.28}$$

It is important to note that the average $\bar{G}_i$ has to be subtracted from the measurement before performing the Fourier transform.

Autocorrelation affects error analysis: it increases the variance on the sample by an amount equal to the *autocorrelation time* s^a. It is defined as

$$s_i^a = \sum_{\delta s=0}^{\infty} \frac{A_i(\delta s)}{A_i(0)}, \tag{2.29}$$

and the variance of the sample becomes

$$\sigma_i^2 = \frac{s_i^a}{M(M-1)} \sum_{j=1}^{M} (G_i^{(j)} - \bar{G}_i)^2. \tag{2.30}$$

This correction affects also the covariance matrix in (3.13). In this work, we opted for a rougher approach: as a rule of thumb, to take autocorrelation into account we simply multiplied the covariance matrix by a factor equal to the timestep ς_i after which autocorrelation drops under a fixed threshold θ. Thus, (3.14) becomes:

$$C_{ik} = \frac{\varsigma_i \varsigma_j}{M(M-1)} \sum_{j=1}^{M} (\bar{G}_i - G_i^{(j)})(\bar{G}_k - G_k^{(j)}). \tag{2.31}$$

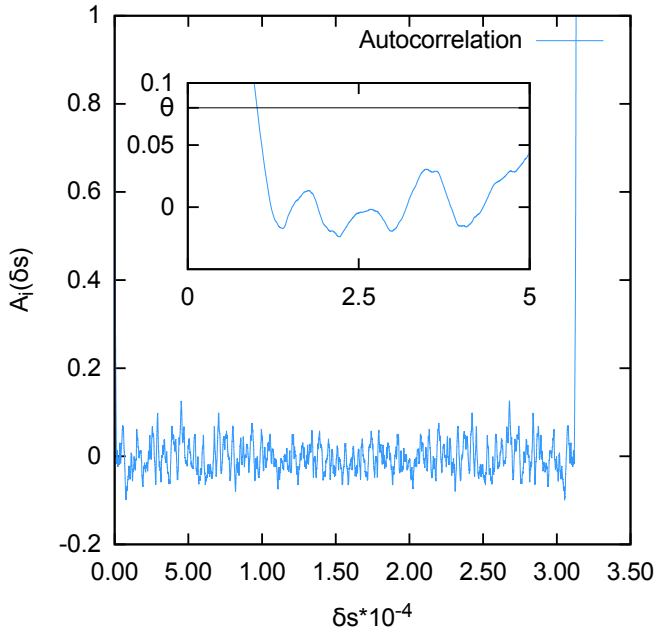

Figure 5: Plot of the autocorrelation for the component $G^{++}(\omega_0)$ with $N_\omega = 32$ vs Monte Carlo time difference. The small panel shows the autoorrelation up to $\delta s = 5 \cdot 10^4$. The function $f = \theta$ is also drawn, to show how the selection for ς_{ω_0} is performed. The periodicity in the autocorrelation is due to the discrete Fourier transform.

3

SPECTRAL RECONSTRUCTION

As mentioned in the introduction, imaginary time correlators and spectral functions are related trough the convolution [15]:

$$G(\tau) = \int d\mu \tilde{K}(\mu, \tau, \beta)\rho(\mu),\ \tilde{K} = \frac{e^{-\tau\mu}}{1 \pm e^{-\beta\mu}}. \tag{3.1}$$

The positive (negative) sign is for fermion (boson) operators. By inverting this relation, in principle one can gain access to the spectral function $\rho(\mu)$, that encodes dynamical information on the physical system in consideration. Typically, a spectral function contains δ-peaks in corresponence to the single-particle mass, so the spectral function has the form

$$\rho(\mu) \sim \delta(\mu - m),\ \text{with } \mu \geq 0. \tag{3.2}$$

and δ-peaks at values of $\mu < 2m^2$

$$\rho(\mu) \sim \delta(\mu - m_1) + \delta(\mu - m_2), \tag{3.3}$$

which are manifestations of bound states. For values of $\mu \geq 2m^2$ continuum structures, signature of multi-particle states arise [1].

When dealing with spectral reconstruction from imaginary time correlator data, one has to struggle with the kernel $\tilde{K}(\mu, \tau\beta)$ in (3.1): at large μ it becomes exponentially small, and, Monte Carlo data usually being incomplete and noisy, large μ features of $\rho(\mu)$ are only partially resolved. Furthermore the explicit inversion of (3.1) involves a two-sided Laplace transform, that is an ill-posed problem.

The data obtained with our simulation prescription are function of imaginary frequency ω, so they are related to the spectral function via the rational Källén-Lehmann ([16],[17]) kernel:

$$G(\omega) = \int d\mu\, K(\mu, \omega)\rho(\mu),\ K(\mu, \omega) = \frac{2\mu}{\mu^2 + \omega^2}. \tag{3.4}$$

According to (3.4), a spectral function of the type (3.2) will produce correlator of the form:

$$G(\omega) = \int d\mu \, \frac{2\mu}{\mu^2 + \omega^2} \delta(\mu - m) = \frac{2m}{m^2 + \omega^2}, \tag{3.5}$$

i.e. a Breit-Wigner peak. In the case of a spectral function like (3.3), the correlator reads:

$$\begin{aligned} G(\omega) = &\int d\mu \, \frac{2\mu}{\mu^2 + \omega^2} \left(\delta(\mu - m_1) + \delta(\mu - m_2)\right) = \\ =&\frac{2m_1}{m_1^2 + \omega^2} + \frac{2m_2}{m_2^2 + \omega^2}, \end{aligned} \tag{3.6}$$

that is a sum of two Breit-Wigner peaks.

The Källén-Lehmann kernel at higher frequency shows polynomial decay, that does not suppress high frequency contributions as strongly as the Laplace kernel, having an exponential decay, thus improving attempts of reconstruction of spectra. Alas, also this spectral representation carries some problems that impede direct inversion, that is to explicitly find the inverse kernel K^{-1}. The first concerns the kernel, it is undefined on the subspace identified by $\omega = 0$:

$$\lim_{\mu \to 0^{\pm}} K(\mu, \omega)_{\omega=0} \sim \frac{1}{\mu} = \pm\infty. \tag{3.7}$$

But this inconvenient is easly circumventable. One can redefine K as:

$$K'(\mu, \omega) = K(\mu, \omega)\mu = \frac{2\mu^2}{\mu^2 + \omega^2}. \tag{3.8}$$

This kernel has better behaviour at $\omega = 0$, except still not being defined at $(0, 0)$. One then imposes the kernel to be $K'(0, 0) = 0$ since the bosonic spectral function has to be antisimmetric, i.e. $\rho(0) = 0$. In order to be consistent, also the spectral function has to be rescaled, henceforth (3.4) becoming

$$G(\omega) = \int d\mu \, K'(\mu, \omega) \frac{\rho(\mu)}{\mu} = \int d\mu \, \frac{2\mu^2}{\mu^2 + \omega^2} \frac{\rho(\mu)}{\mu}. \tag{3.9}$$

Inverting this equation gives the rescaled spectral function $\rho'(\mu) := \frac{\rho(\mu)}{\mu}$, from which the physical one is easly obtainable.

A more fundamental problem lies in the fact that the correlator $G(\omega)$ is computed trough a Monte Carlo technique. This means that, even though the datapoints fit to the expected function, one does not have their exact functional form, thus making the direct inversion meaningless. To overcome this last difficulties authors relied, for example, on the Padé approximation [3], used to approximate the analytic continuation of the datapoints.

In this work we opted for a Bayesian inference based method: it selects the most likely spectral function using as criterium the maximization of the posterior probability.

In this chapter we will explain the basics of Bayesian inference, and explain in detail the spectral reconstruction method.

BAYESIAN INFERENCE

The aforementioned Bayesian strategy relies on the maximization of the posterior probability, that is the probability of a specific spectral function $\rho(\mu)$ having certain $G(\omega)$ as simulated correlator. Those quantities are connected via the Bayes theorem [18]. Given two events a and b, the theorem says:

$$P[a,b] = P[a|b]P[b] = P[b|a]P[a]. \tag{3.10a}$$

$$\implies P[a|b] = \frac{P[b|a]P[a]}{P[b]} \tag{3.10b}$$

$P[a,b]$ is the joint probability of the two events, and $P[a|b]$ and $P[b|a]$ are conditional probabilities for the realization of a given b and vice versa. $P[a|b]$ is called *posterior probability*, $P[b|a]$ is the *likelihood*, $P[a]$ is the *prior probability* and $P[b]$ is the *evidence*. The evidence is just an irrelevant constant.

BAYESIAN SPECTRAL RECONSTRUCTION

Identifying the a and b with the functions $\rho(\mu)$ and $G(\omega)$, (3.10) reads:

$$P[\rho|G] = \frac{P[G|\rho]P[\rho]}{P[G]}. \tag{3.11}$$

Assuming a uniform prior probability ($P[\rho] \sim$ const), our initial criterion to select the "best" spectral function is that of maximum likelihood. The likelihood is a distribution function of the data that depends on a set of parameters; and the maximum likelihood prescribes a maximization of this distribution with respects to the parameters. Is a type of parameter fitting problem.

After discretizing the μ-axis in N_μ with spacing $\Delta\mu$, the spectra $\rho(\mu_l) = \rho_l$, $l = 1, ..., N_\mu$, are taken as the set of parameters. The maximum likelihood method prescribes to vary ρ so that the resulting G maximizes some likelihood function. The method does not specify the likelihood function, but most of the times is specified by he physical system under examination. But, as the central limit theorem argues, the asymptotic behaviour of the likelihood becomes:

$$e^{-L} = e^{-\chi^2/2}, \tag{3.12}$$

with L the logarithm of the likelihood function. χ^2 is given by

$$\chi^2 = \sum_{i,j}^{N_\omega} (\bar{G}_i - G_i^\rho) C_{ij}^{-1} (\bar{G}_j - G_j^\rho). \tag{3.13}$$

C is the covariance matrix:

$$C_{ik} = \frac{1}{M(M-1)} \sum_{j=1}^{M} (\bar{G}_i - G_i^{(j)})(\bar{G}_k - G_k^{(j)}). \tag{3.14}$$

G_j^ρ is the $j-$th component of the ideal two-point function, calculated trough (3.4). $\bar{G}_k$ is the Monte Carlo-average of the k-th component of the two-point function. $G_j^{(j)}$ is the $j-$th measurement of the $k-$th componentof the two-point function.

Under Gaussian hypotesis, maximizing the likelihood is equivalent to minimizing χ^2, that is the well known least-squares fitting procedure.
The maximum likelihood is useful in problems involving few parameters; but in our case N_μ is much larger than N_ω, so the likelihood doesn't provide a sufficient contraint for the parameters. This eventually leads to overfitting ($\chi^2 \approx 0$), with noisy and non unique results.
To overcome this problem, is sufficient to note a simple fact: the spectral function $\rho(\mu)$, in many cases, is normalizable to unity and is non-negative. This opens to an interpretation of such as a probability distribution. In this framework, the prior probability is not constant, but it obeys the distribution given by $\rho(\mu)$. The probability distribution $\rho(\mu)$ then is the one that maximizes the Shannon-Jaynes entropy. This method is a particular implementation of the Bayesian strategy, called Maximum Entropy method. The entropy acts as a regulator, that allows to select between the many equilikely solutions. The Shannon-Jaynes entropy depends on prior information I, i.e. the spectral function in absence of data. Taking into account the prior information, Bayes theorem reads

$$\begin{aligned} P[\rho, G, I] =& P[\rho|G, I]P[G, I] = P[G|\rho, I]P[\rho, I] \\ \implies & P[\rho|G, I]P[G|I]P[I] = P[G|\rho, I]P[\rho, I]P[I] \\ \implies & P[\rho|G, I] = \frac{P[G|\rho, I]P[\rho|I]}{P[G|I]}, \end{aligned} \tag{3.15}$$

where the fact that $P[I] = 1$ is explicitly used. The prior probability is now found to be:

$$P[\rho|I] \propto e^{\alpha S}. \tag{3.16}$$

α is a hyperparameter, adjustable such that $\chi^2 = N_\omega$. A specific form of the entropy functional is selected by stating four axioms, specifying the properties of the entropy: subset in-

dependence, coordinate invariance, system independence and scaling. The function S has then the form:

$$S = \int d\mu \left(\rho(\mu) - m(\mu) - \rho(\mu) \ln \left[\rho(\mu)/m(\mu)\right]\right). \tag{3.17}$$

Now it's clear under our hypoteses (gaussianity and interpretation of spectral function as probability function) that the maximum entropy method deals with the maximization of $Q = \alpha S - \frac{1}{2}\chi^2$ with respect to $\rho(\mu)$.

One can easily show that:

$$\frac{\delta^2 S}{\delta\rho_i \delta\rho_j} = \frac{-\delta_{ij}}{\sqrt{\rho_i \rho_j}}. \tag{3.18}$$

This tells us that the entropy is a concave function of the ρ_i. Since χ^2 is also a concave funtction of the ρ_i, so is $Q = \alpha S - \chi^2$. Consequently, Q has a unique maximum, at fixed α.

The maximum entropy method assumes normalizability and non-negativeness of the spectral function; that may be true for a bosonic system, but in general is not (e.g. gauge theories [19]); so not always the spectral function can be interpreted as a probability function. In this work we hand-picked four axioms [20] in order to construct a new regulator. The ones used to build it are:

SUBSET INDEPENDENCE Considering two subsets of the frequency domain Ω_1 and Ω_2; if the prior information constraints the spectrum ρ on each of these subsets, then the result does not change if these subsets are considered separately, i.e. $S[\Omega_1, \Omega_2, m(\Omega_1), m(\Omega_2)] = S[\Omega_1, m(\Omega_1)] + S[\Omega_2, m(\Omega_2)]$, or combined, i.e. $S[\Omega_1, \Omega_2, m(\Omega_1), m(\Omega_2)] = S[\Omega 1 \cup \Omega_2, m(\Omega_1 \cup \Omega_2)]$. This is satisfied if the regulator has the form:

$$S \propto \int d\mu\, s(\rho(\mu), m(\mu), \omega). \tag{3.19}$$

The maximum entropy method already needs this axiom, since it is equivalent to the additivity of the entropy.

SCALE INVARIANCE Since $\rho(\mu)$ does not have to be a probability function, its scaling is not always $1/\omega$. Hence, the units of $\rho(\mu)$ and $m(\omega)$ should not interfere with the reconstruction, i.e. the regulator should be function of the ratio $r = \rho/m$ only:

$$S(r) = \tilde{\alpha} \int d\mu \, s(\rho(\mu)/m(\mu)). \tag{3.20}$$

SMOOTHNESS OF THE SPECTRA The only information about the spectral function is that is smooth and positive definite. Thus, regardless of the prior $m(\omega)$ the reconstruction should select a smooth spectrum. The implementation of such relies on penalization of spectra such that variations of the ratio $r_n = \rho_n/m$ between adjacent frequencies ω_n and ω_{n+1} does not vary G^ρ beyond errorbars. In this case S should then favor spectra such that $r_n = r_{n+1} := r$. The penalty between the cases $r_n = r_{n+1} = r$ and the case where they differ for a small amount $r_n = r(1+\varepsilon)$, $r_{n+1} = r(1-\varepsilon)$ has to be r-independent and symmetric:

$$2s(r) - s(r(1+\varepsilon)) - s(r(1-\varepsilon)) = \varepsilon^2 C_2. \tag{3.21}$$

This is the discretized expression of $-r^2 s''(r) = C_2$, that has as solution:

$$S = \tilde{\alpha} \int d\mu \left(C_0 - C_1 \frac{\rho}{m} + C_2 \frac{\rho}{m} \right). \tag{3.22}$$

MAXIMUM AT THE PRIOR The regulator should be maximum at $\rho = m$ in absence of data. Conventionally, one choses the regulator to vanish when $r = 1$:

$$S(1) = 0; \quad S'(1) = 0; \quad S''(1) < 0. \tag{3.23}$$

The first two conditions fix the constants C_0, C_1 and C_2 to an overall factor that can be absorbed in the hyperpatameter $\alpha \propto \tilde{\alpha}$. The third imposes positivity on α .

Thus, the final results is:

$$S = \alpha \int d\mu \left(1 - \frac{\rho}{m} + \ln \frac{\rho}{m} \right). \tag{3.24}$$

This form of the prior probabilit distribution is concave ($S \leq 0$) and has a maximum at $\rho = m$, properties shared also by the Shannon-Jayes entropy. Analogously to the Shannon-Jaynes entropy, one can prove the concavity of S in ρ-space, and thus the uniqueness of a maximum of Q.

RECONSTRUCTION SETUP

The task of inverting (3.4) starts with the discretization of $\rho(\mu_l) = \rho_l$ over frequencies μ_l using N_μ points, in the frequency window $\mu \in [0, \mu_{MAX}]$. μ_{MAX} is arbitrary and needs to be chosen appropriately, to take into account all the relevant structures in the spectral function.

The discretized version of (3.4) reads:

$$G_i = \Delta\mu \sum_{l=1}^{N_\mu} K'_{il}\rho'_l, \tag{3.25}$$

where the integral is approximated with quadrature. K'_{il} is the discrete modified Källén-Lehmann kernel (3.8), and ρ'_l is the rescaled spectral function. As mentioned in §3.2, the method is based on maximization of posterior probability $P[\rho|G] = e^{-Q}$, with:

$$\begin{aligned} Q &:= \frac{1}{2}\chi^2 - \alpha S + \\ &= \frac{1}{2}\sum_{i,j}^{N_\omega}(\bar{G}_i - G_i^\rho)C_{ij}^{-1}(\bar{G}_j - G_j^\rho) + \\ &+ \alpha \int d\mu \left(1 - \frac{\rho}{m} + \ln\frac{\rho}{m}\right). \end{aligned} \tag{3.26}$$

G_i^ρ is calculated trough (3.25), where ρ'_μ is parametrized as $\rho'_\mu = m_\mu \exp\{a_\mu\}$, to explicit positive definiteness and smoothness of the spectrum.

The regulator is also approximated with simple quadrature:

$$\int d\mu \left(1 - \frac{\rho(\mu)}{m(\mu)} + \ln\frac{\rho(\mu)}{m(\mu)}\right) \approx \Delta\mu \sum_{\mu=1}^{N_\mu} \left(1 - \frac{\rho_\mu}{m_\mu} + \ln\frac{\rho_\mu}{m_\mu}\right). \tag{3.27}$$

The suffix μ was used to emphasize the nature of $\rho(\mu)$ and $m(\mu)$ of vectors. To reduce computation time calculations were per-

formed in a basis where the covariance matrix (3.14) is diagonal. The final form of the posterior probability is then:

$$\begin{aligned} Q(\alpha) = \frac{1}{2}\sum_{i=1}^{N_\omega}(\bar{G}_i - G_i^\rho)^2 C_{ii}^{-1} + \\ - \alpha\Delta\mu \sum_{\mu=1}^{N_\mu}\left(1 - \frac{\rho_\mu}{m_\mu} + \ln\frac{\rho_\mu}{m_\mu}\right) \end{aligned} \tag{3.28}$$

Maximization of the posterior probability is equivalent to the minimization of Q with respect to $\rho(\mu)$. This task is then equivalent to the minimization of the discretized Q with respect to the parameters a_μ. Thus the problem can be stated as finding the set of parameters $\{a_\mu\}$ such that

$$\frac{\partial Q}{\partial a_\mu} = 0, \tag{3.29}$$

for an initial guess value for α; the resulting parameter $\{a_\mu\}(\alpha)$ will be then α-dependent. As mentioned in chapter 3, depending on the value of α overfitting or underfitting may occurr. Thus, α has to be manually adjusted in order to satisfy $L(\alpha) = N_\omega$. This was efficiently accomplished via simple bisection: the central part of the spectral reconstruction algorithm consists in solving the equation $L(\alpha) - N_\omega = 0$ in a window $[0, \alpha_{MAX}]$, and every function evaluation requires a minimization (3.29), which provides with a parameter set $\{a_\mu\}(\alpha_c)$ tied to the current α_c guess. The minimization is performed deploying an optimized version of the Broyden-Fletcher-Goldfarb-Shanno (BFGS) algorithm [21]. The spectral function is then calculated via:

$$\rho_\mu = \mu\rho'_\mu = \mu m_\mu e^{a_\mu}. \tag{3.30}$$

Again, to recap, here is the scheme for the spectral reconstruction algorithm:

1. Read single realizations of observable $G^{(j)}$ and calculate average $\bar{G}$;

2. Calculate coefficients ς_i trough autocorrelation computation;

3. Select window in α-space $[0, \alpha_{MAX}]$ and start with the bisection, using as the first guess $\alpha_C = \alpha_{MAX}/2$;

4. Calculate $L(\alpha_C)$ trough minimization, if $L(\alpha_C) < 0$ then the new window becomes $[\alpha_C, \alpha_{MAX}]$, otherwise $[0, \alpha_C]$. If $L(\alpha_C) = 0$ the algorithm stops;

5. Repete point 4. until $L(\alpha_C) - N_\omega < \varepsilon$, with $\varepsilon \ll 1$ arbitrary threshold, and obtain the "best" parameter set $\{a_\mu\}(\alpha_C)$;

6. Calculate spectral function using (3.30).

The method was tested on mock data, generated from two ideal specral functions: one presenting one peak structure $\rho_1(\mu) = \delta(\mu - m^2)$ and the other with a two-peak structure $\rho(\mu) = \delta(\mu - m_1^2) + \delta(\mu - m_2^2)$. The mock-correlator $\bar{G}^{mock}$ was calculated using (3.4), and to compute the covariance matrix fake measurement were generated by adding Gaussian distributed numbers to the mock-correlator, with standard deviation

$$\sigma_i^{mock} = K \bar{G}_i^{mock} \sqrt{M}. \tag{3.31}$$

K is a prefactor, chosen to be 10^{-4}.

In figure 6 the data and results are shown. Manifest is the difference in height in the two-peaks case between the mock peaks and the reconstructed ones; this difference is meaningless, since it doesn't hold any phisical information. The only feature we're after is the position, that is related to the mass of the simulated particle/s. The two mock spectrum have respectively peaks at $\mu = 1$ and $\mu_1 = 0.5$, $\mu_2 = 1$. The first reconstructed spectrum shows a peak at $\mu = 1.004$, the second shows peaks at $\mu_1 = 0.493$ and $\mu_2 = 0.995$, thus with relative differences respectively of 0.4%, 0.7%, and 0.5%.

Errorbars

Errorbars on fit parameters can be calculated using the jackknife resampling method [22]. It is used to estimate the variance of a set of parameters $\{a_\mu\}$. Let's suppose one has a

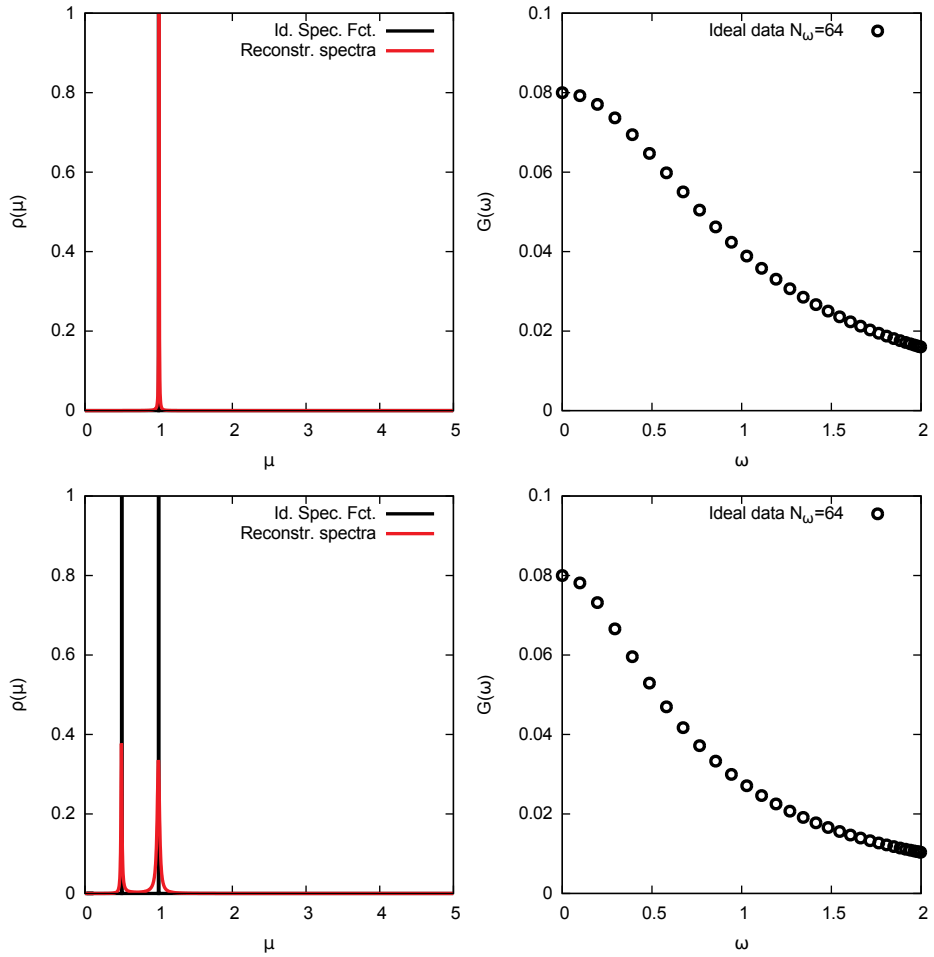

Figure 6: Left column: ideal (grey) and reconstructed (black) spectral functions, with respectively one and two δ-peaks. Right column: Mock data generated from the ideal spectral function to their left.

dataset $G = \{G^{(0)}, G^{(1)}, G^{(2)}, ..., G^{(M)}\}$ and one proceeds to fit the dataset via a parameter set $\{a_\mu\}$, for example, through a spectral reconstruction algorithm. However, those parameters have to be evalueted with respect to the "real" ones $\{a_{real}\}$, unknown to the experimenter, i.e. one needs errorbars. The jackknife provides a reliable tool to achieve this goal. The starting point is to choose a binsize on lenght n. Then one needs to subtract from the dataset the first n measurements, fit them and find another parameter set $\{a_\mu\}_1 = \{a_0^1, a_1^1, a_2^1, ...\}$. The next step is the same, but one needs to remove from the dataset the second n measurements, that is the one from $n+1$ to $2n$, and find the set of parameters $\{a_\mu\}_1 = \{a_0^2, a_1^2, a_2^2, ...\}$. And so on un-

til every measurement is included in one of the removed bins. The new sets of parameters $\{a_\mu\}_i$, with $i = 1, ..., M/n$, are then used to estimate the variance of the original parameter set $\{a_\mu\}$ with

$$\sigma_{a_\mu} = \sqrt{\frac{M-1}{M} \sum_{j=1}^{M} \left(a_\mu - a_\mu^j\right)^2} \tag{3.32}$$

4

TOWARDS BOUND STATES IN 2+1D φ^4 SCALAR THEORY

SYMMETRIC THEORY REVIEW

Before showing the results in the broken symmetry phase of the scalar field, a review of the results in the symmetric phase is in order.

To test the imaginary frequency simulation prescription we performed simulations of real scalar field theory in the symmetric phase, on a 2+1-dimensional lattice, both in the free case and with φ^4 interactions.

We performed the simulations on a lattice $\Lambda = N_p^2 \times N_\omega$, where $N_p = 32$ and $N_\omega = 32, 64, 128, 256$, computing the correlator $G^{++}(\omega)$. The simulated theory has a mass parameter $m^2 = 1$ and, in the interacting case, coupling constant $\lambda = 24$. A Breit-Wigner fit is also shown, to check that the simulation results behave accordingly to (3.5). We generated a total of 10^5 field configurations, used to compute as many individual correlator measurements. In both cases, the corresponding spectral function should be a δ-peak, because in the symmetric phase we don't expect bound states to appear, thus the only structure in the spectral function is the peak corresponding to the ground state mass of the simulated field. In the free case it position corresponds to the rest mass of the simulated field, in the other case interactions give rise to a higher mass, thus positioning the peak in a higher frequency zone. As previously noted, this feature can be connected to the analytical form of the correlator via (3.5) and (3.6). Since our observable is the result of a Monte Carlo simulation we don't know its functional form, but a fit will suffice. We included in Fig 7 also the Breit-Wigner fit of both correlator; as one can see the fit reproduces

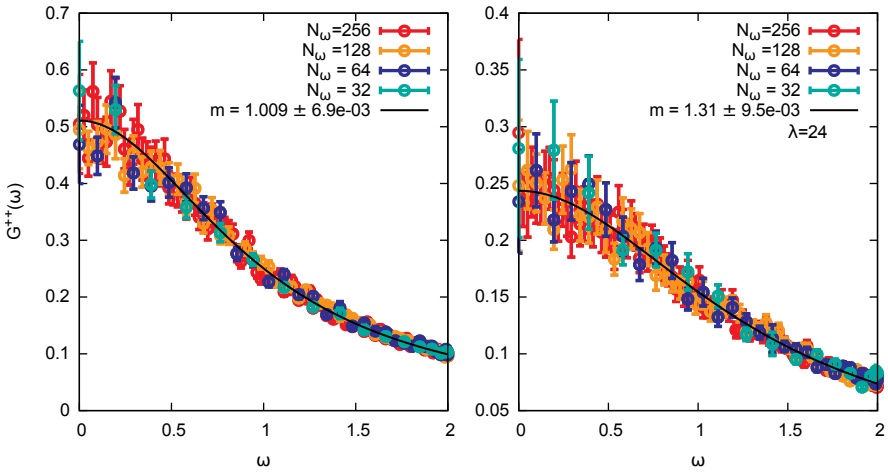

Figure 7: Top: Imaginary frequency correlator $G^{++}(\omega)$ at $\lambda = 0$, at different lattice sizes. Bottom: Same observable, with $\lambda = 24$. The black line corresponds to the Breit-Wigner peak.

the data within errorbars. The error on the mass parameter is given by the χ^2 minimization.

In Fig. 8 are shown the corresponding extracted spectral functions. The functions was parametrized using $N_\mu = 7500$ points, defined on the frequency window $\mu \in [0, 10]$.

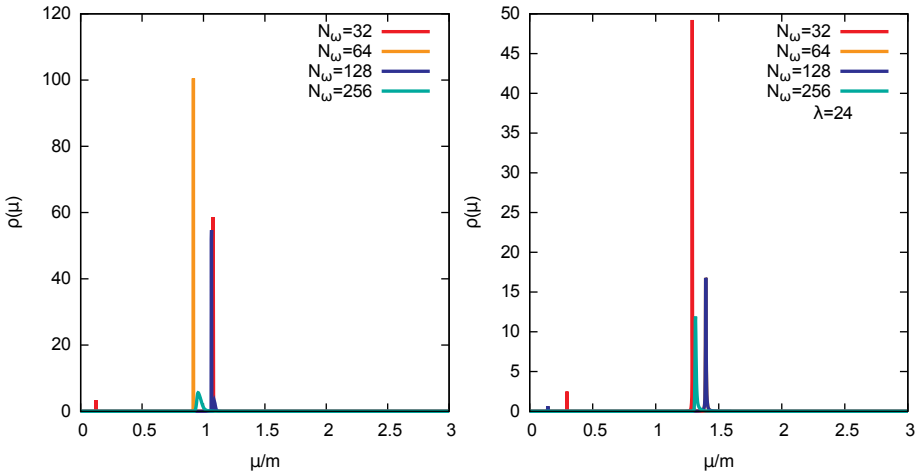

Figure 8: Reconstructed spectral functions from correlators in the symmetric phase, using different resolutions on the ω-direction. Left: free theory. Right: interacting theory with $\lambda = 24$

In Fig. 8 the frequency window was shrunk in order to appreciate more the differences between the reconstructed peaks.

As one can see, in the spectral functions extracted from low-resolution correlators secondary peaks are present. This is a manifestation of a systematical understatement of systematic error from the Bayesian reconstruction method. Fig. 8 shows the best estraction we could achieve, i.e. the Likelihood produced by the parameter set $\{a_\mu\}$ shown in Fig. 8 was as close as possible to the number of datapoints N_ω composing the correlator. For each of these reconstructions the Likelihood was always higher than expected, thus leading to underfitting. Nonetheless, the position of the highest peak mirrors the mass extracted from the Breit-Wigner fit, confirming its result.

BROKEN SYMMETRY PHASE SIMULATION

To simulate in the broken symmetry phase, it's sufficient to use a negative squared mass in the action. In this way the action becomes

$$S \supset -m^2\varphi^2 + \frac{\lambda}{4!}\varphi^2, \tag{4.1}$$

that is the well-known "mexican hat" potential. The $\mathbb{Z}_2$ symmetry of the scalar field imposes a zero macroscopic field: $\langle\varphi\rangle = 0$; in the broken phase the macroscopic field becomes non-zero, being the minimum of the potential (4.1) not zero.

In the broken symmetry phase simulation results are affected by wriggly structures, impeding Breit-Wigner fit of the correlator data. Similar structures were observed also in simulation results of gauge theories, being reduced only with really high statistics. During the time frame of this project developement was not possible to collect enough statistics to dampen the effect of such structures.

Simulations were performed on a 2+1-dimensional periodic lattice of $32^2 \times 64$ points. The simulated fields have a mass of $m^2 = -5$. The coupling constant was set to be $\lambda = 1$. A total of 10^5 individual measurements were collected. The results are shown in Fig. 9.

The fit shown in Fig. 9 is not reliable, beside from the obvious fact that the data does not agree with the fit inside error-

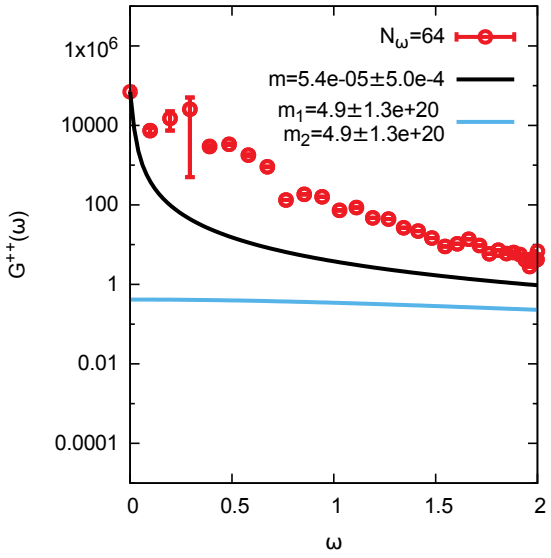

Figure 9: Correlator in the broken symmetry phase for $N_\omega = 64$. The black line is the single Breit-Wigner fit, the blue one is the double Breit-Wigner fit.

bars, because the standard deviation on the parameters (found through a χ^2-minimization is very high, as shown in the plot key.

From the correlator in Fig. 9 we tried to extract a $N_\omega = 32$ correlator, by averaging neighboring values.

Alas, also we cannot extract a significant mass parameter from this correlator.

Even though we could not extract a significant mass parameter from the Breit-Wigner fit, we can nonetheless infere physical information from the data, via spectral reconstruction, as shown in the next section.

BOUND STATE SIGNATURES

Signatures of bound states can be read in the spectral function, as mentioned in the introduction. As shown in [3], the presence of bound states is stated by two δ-peaks. As one would expect, interactions produce a shift in the mass. The authors show that in the presence of bound states, this shift occurs towards the

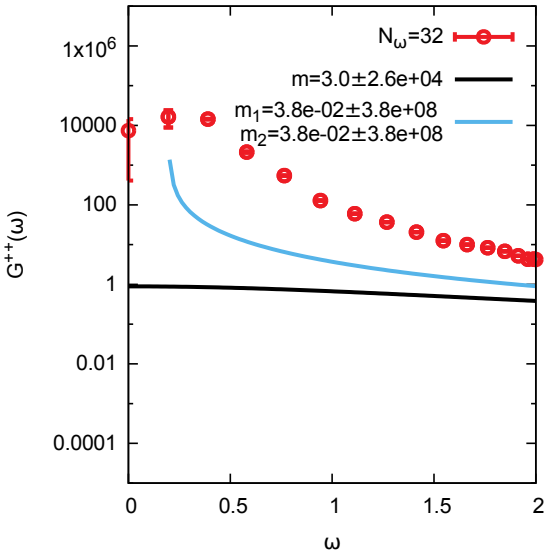

Figure 10: Correlator in the broken symmetry phase for $N_\omega = 32$, obtained from correlator in Fig. 9 by averaging neighboring values.

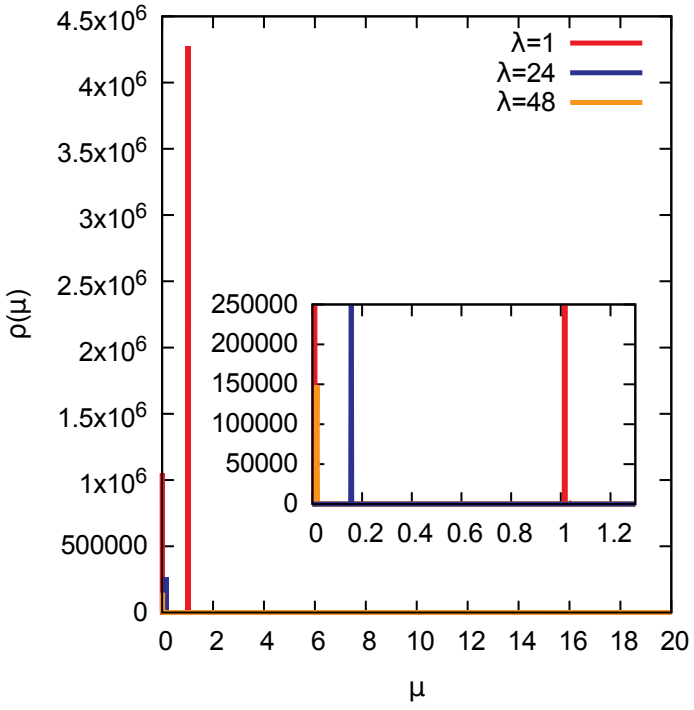

Figure 11: Extracted spectral functions from broken phase correlators, with different coupling constants λ.

low frequency spectrum. To test this behaviour we produced simulation data on a lattice of dimension $32^2 \times 64$, varying the coupling constant, using $\lambda = 1,\ 24,\ 48$. We observed a radical

shift of the peak position towards the lower frequencies when increasing the coupling constant. Reconstruction were carried out using $N_\mu = 7500$ parameters to fit the spectral function to, defined on the frequency window $\mu \in [0, 20]$.

The second peak was not resolved by the reconstruction, but we could show the shifting towards the lower frequency part of the spetrum. This shifting increases with the coupling strenght. We believe that this is indeed an evidence of the presence of this first bound state of the theory of the theory.

CONCLUSIONS

In this work we aimed to collect numerical clues regarding the presence of the first bound state in the broken symmetry phase of the real scalar φ^4 theory, fromcorrelators simulated with the new imaginary frequency simulation prescription, with field configurations generated via stochastic quantization. The clues were read from the spectral function extracted with Bayesian reconstruction from the simulated correlators.

In the first place, we tested the imaginary frequency simulation prescription in the symmetric phase of the 2+1-dimensional real scalar field theory, both free and with φ^4 interactions. Results in this framework were positive, since they fitted to a Breit-Wigner peak as expected, from which the simulated mass parameter was correctly extracted. Also we recorded the peak shift to higher frequencies due to interactions.

The extracted spectral functions from the symmetric phase data showed structures corresponding to the expected peaks, confirming the mass extraction from the Breit-Wigner peak (result anticipated by the spectral reconstruction on mock data). Even though underfitting tends to occur, there's already good agreement between the numerical result and the theoretical prediction.

Simulations in the broken phase were performed, to investigate clues of the presence of the first bound state, but the simulated correlators show too many wriggly structures to obtain a reliable fit. From neither of the $N_\omega = 64$ correlator and the one obtained by averaging neighboring values, having $N_\omega = 32$ we could extract a significant mass parameter from the Breit-Wigner fit.

Spectral reconstruction on correlator with $N_\omega = 64$ and different coupling constants showed positive results: even though we could not resolve the second peak in the spectral function,

we confirmed the mass shifting towards the low frequency part of the spectrum, as expected. This shifting was shown to increase with higher coupling constants. This was interpreted as a positive clue regarding the presence of the bound state in the theory.

BIBLIOGRAPHY

[1] M. E. Peskin and D. V. Schroeder, *An Introduction To Quantum Field Theory.* Westview Press, 1995.

[2] M. Caselle, M. Hasenbusch, P. Provero, and K. Zarembo, "Bound states in the three dimensional phi^4 model," jan 2000.

[3] F. Rose, F. Benitez, F. Léonard, and B. Delamotte, "Bound states of the ϕ^4 model via the nonperturbative renormalization group," *Phys. Rev. D*, vol. 93, p. 125018, jun 2016.

[4] Y. Nishiyama, "Universal critical behavior of the two-magnon-bound-state mass gap for the (2+1)-dimensional Ising model," *Physica A: Statistical Mechanics and its Applications*, vol. 413, pp. 577–582, nov 2014.

[5] V. Agostini, G. Carlino, M. Caselle, and M. Hasenbusch, "The Spectrum of the 2+1 Dimensional Gauge Ising Model," jul 1996.

[6] P. Fonseca and A. Zamolodchikov, "Ising Field Theory in a Magnetic Field: Analytic Properties of the Free Energy," *Journal of Statistical Physics*, vol. 110, no. 3/6, pp. 527–590, 2003.

[7] J. M. Pawlowski and A. Rothkopf, "Thermal dynamics on the lattice with exponentially improved accuracy," *Physics Letters B*, vol. 778, pp. 221–226, mar 2018.

[8] J. Berges, "Nonequilibrium Quantum Fields: From Cold Atoms to Cosmology," mar 2015.

[9] J. Smit, *Introduction to Quantum Fields on a Lattice*. Cambridge: Cambridge University Press, 2002.

[10] K. Temme, T. J. Osborne, K. G. Vollbrecht, D. Poulin, and F. Verstraete, "Quantum Metropolis sampling," *Nature*, vol. 471, pp. 87–90, mar 2011.

[11] M. Namiki, *Stochastic Quantization*. Springer Publishing Company, Incorporated, 1st ed., 2013.

[12] W. H. Press, *Numerical recipes : the art of scientific computing*. Cambridge University Press, 2007.

[13] A. S. Kronfeld and A. S., "Dynamics of Langevin Simulation," *Progress of Theoretical Physics Supplement, No. 111, pp. 293-311*, vol. 111, pp. 293–311, may 1992.

[14] P. F. Dunn, *Measurement and data analysis for engineering and science*. CRC Press/Taylor & Francis, 2010.

[15] M. Jarrell and J. Gubernatis, "Bayesian inference and the analytic continuation of imaginary-time quantum Monte Carlo data," *Physics Reports*, vol. 269, pp. 133–195, may 1996.

[16] G. Källén, "On the definition of the Renormalization Constants in Quantum Electrodynamics," *Helv. Phys. Acta*, vol. 25, no. 4, p. 417, 1952.

[17] H. Lehmann, "Über Eigenschaften von Ausbreitungsfunktionen und Renormierungskonstanten quantisierter Felder," *Il Nuovo Cimento*, vol. 11, pp. 342–357, apr 1954.

[18] C. M. Bishop, *Pattern Recognition and Machine Learning (Information Science and Statistics)*. Secaucus, NJ, USA: Springer-Verlag New York, Inc., 2006.

[19] F. Strocchi and F., *Selected Topics on the General Properties of Quantum Field Theory*, vol. 51 of *World Scientific Lecture Notes in Physics*. World Scientific Publishing Co. Pte. Ltd., 1993.

[20] Y. Burnier and A. Rothkopf, "Bayesian Approach to Spectral Function Reconstruction for Euclidean Quantum Field

Theories," *Physical Review Letters*, vol. 111, p. 182003, oct 2013.

[21] R. Fletcher, *Practical methods of optimization*. Wiley, 1987.

[22] B. Efron and C. Stein, "The Jackknife Estimate of Variance."

ERKLÄRUNG

Ich versichere, dass ich diese Arbeit selbstständig verfasst habe und keine anderen als die angegebenen Quellen und Hilfsmittel benutzt habe.

Heidelberg, den 20/04/2018 .....